Modeling the Decomposition Signal and Correcting Bulk Organic Data From a Peat Deposit, a Case Study at Low Latitudes (Cameroon)

Valentine Schaaff, David Sebag, Matthew Makou, Vincent Grossi, Ingrid Antheaume, Bruno Hamelin, Yannick Garcin, Benjamin Ngounou Ngatcha, Pierre Deschamps, Guillemette Ménot

Modeling the decomposition signal and correcting bulk organic data from a peat deposit, a case study at low latitudes (Cameroon)

Valentine Schaaff[1], David Sebag[2], Matthew Makou[1], Vincent Grossi[1], Ingrid Antheaume[1], Bruno Hamelin[3], Yannick Garcin[3], Benjamin Ngounou Ngatcha[4], Pierre Deschamps[3], Guillemette Ménot[1]

[1] Université de Lyon, ENS Lyon, UCBL, CNRS, UMR 5276 LGL-TPE, 69364 Lyon, France

[2] IFP Energies Nouvelles, Earth Sciences and Environmental Technologies Division, 1 et 4 Avenue de Bois-Préau, 92852 Rueil-Malmaison, France

[3] Aix-Marseille Université, CNRS, IRD, Collège de France, Centre Européen de Recherche et d'Enseignement des Géosciences de l'Environnement UM34, 13545 Aix-en-Provence, France

[4] Department of Earth Sciences, Faculty of Sciences, University of Ngaoundéré, Ngaoundéré, Cameroon

Corresponding author: Valentine Schaaff valentine.schaaff@ens-lyon.fr

Abstract

Organic compounds are widely used for paleoclimatic and paleoenvironmental reconstructions. Bulk organic proxies, however, are more complicated to interpret due to the multiple causes of variation in climatic and environmental conditions and the degree of diagenetic alteration. As labile compounds, rich in easily degradable function and generally richer in heteroatoms such as oxygen and nitrogen, decompose, the remaining organic matter becomes progressively richer in refractory carbon and its carbon content increases. Thus, in a peat deposit composed almost entirely of organic matter, total organic carbon (TOC) is expected to increase with time and depth, which could mask the paleoclimatic signal. We propose a simple model for peat sediments to remove the decomposition signal based on a logarithmic function fitted with a partial dataset where decomposition is the main parameter. The subtraction of the obtained logarithmic function to the raw data (i.e., measured data) leads to "residual" data. We discuss the influence of different parameters (water table depth, vegetation, microbial community) on the "residual" data and their possible link to paleoclimatic and paleoenvironmental variations. This method is tested on bulk elemental and isotopic data obtained from a new peatcore from the Adamawa Plateau (North-East Cameroon) covering nearly 10 ka cal BP. Comparison with Rock-Eval® parameters highlights similar variations between the Hydrogen Index and residual TOC variations, supporting the interpretation based on residual TOC. Our approach allows to extract paleoenvironmental information from decomposition-prone bulk organic proxies and can be generalized to peat deposits where decomposition plays a major role in controlling bulk data.

Key words: Peat deposit, Decomposition model, Bulk organic data

Introduction

Paleoclimatic proxies based on organic compounds rely on the assumption that these compounds are resistant to diagenesis. Many organic compounds can record pre-depositional and syn-depositional information such as climatic conditions (e.g., temperature, hydrology) or environmental conditions (e.g., major vegetation types, pH, methanogenesis) (Sachse et al., 2012; Diefendorf and Freimuth, 2017; Inglis et al., 2019; Naafs et al., 2019). This signal can, however, be overprinted by post-depositional processes such as decomposition (Gupta and Kawahata, 2006) or contamination by other reservoirs (Makou et al., 2018).

Peat deposits have been successfully used to reconstruct past climatic variations at all latitudes using diverse proxies such as pollen, plant macrofossils or biomarkers (e.g., Pancost et al., 2003; Booth et al., 2004; Baker et al., 2014). Bulk analysis of organic matter such as Rock-Eval® or elemental analysis are routine techniques in paleoenvironmental studies. These non-specific analyses give first insights into the sources, nature and decomposition stage of organic matter (e.g., Talbot and Johannessen, 1992; Kuhry and Vitt, 1996; Baker et al., 2014). However, in bulk organic data, the paleoclimatic or paleoenvironmental signal is often hidden by the signal of decomposition (Kuhry and Vitt, 1996; Drollinger et al., 2019). Some proxies were specifically developed to reconstruct the peat decomposition stage such as colorimetric determination (Chambers et al., 2011; Biester et al., 2014) or thermal analyses (Upton et al., 2018; Cooper et al., 2019), while others such as the C/N ratio are sometimes used as an indicator of organic matter decomposition (Kuhry and Vitt, 1996) or of organic matter sources (Baker et al., 2014). In intertropical regions, peat deposits have a large paleoclimatic potential especially when applying organic geochemistry techniques (e.g., Sukumar et al., 1993; Bonnefille et al., 1995; Aucour et al., 1996, 1999; Behling and Safford, 2010). Until now, no study has specifically focus on correcting bulk organic data in tropical peat.

Peatlands are highly impacted by organic matter decay (Clymo, 1984). Peats are usually divided in two distinct layers: the upper layer (the acrotelm), above the mean water table depth and exposed to oxic conditions, and the lower layer (the catotelm) situated under the mean water table depth and dominated by anoxic conditions (Ingram, 1978; Clymo, 1984). Clymo (1984) and Clymo et al. (1998) focused on models of peat mass accumulation and decay rules and indicated that about 90% of the original biomass is lost in the upper oxic part of the peat within an indicative period of 10 to 100 years but selective decay continues in the anoxic layer.

Peat organic matter is often mainly composed of different pools of organic compounds with different sensitivities to decomposition (Dodla et al., 2012) and different $\delta^{13}C$ composition (Benner et al., 1987). The labile organic compounds such as carbohydrates and proteins composed of easily hydrolyzable functions rich in oxygen and nitrogen rapidly decompose after deposition while recalcitrant organic compounds such as lignin and lipids, having long carbon chains and aromatic structures rich in carbon, can be selectively preserved (Dodla et al., 2012; Wang et al., 2015). Thus, despite global mass loss and carbon loss during organic matter decomposition (Clymo, 1984), the remaining organic matter, mainly composed of recalcitrant compounds, becomes more and more concentrated in carbon with increasing time and depth (Fig. 1). In the oxic layer, aerobic decomposers preferentially use ^{12}C, resulting in an increase in ^{13}C content (Ågren et al., 1996; Drollinger et al., 2019). The mineral fraction in the peat is a key point to understand the variations in TOC. If the mineral component is very low, the TOC will follow the trend of the organic matter and increase with depth and time (e.g., Upton et al., 2018). In mineral-rich peat, or when mineral fraction supply varies, the increasing trend will no longer be visible because the increasing proportion of the mineral fraction due to the decomposition of the organic matter will mask the evolution of the carbon in the organic matter (e.g., Baker et al., 2014; Njagi et al., 2021).

While the effects of early diagenesis on $\delta^{13}C$, $\delta^{18}O$ or Mg/Ca of foraminifera and carbonate sediments have been studied for decades (Berner, 2020), and several corrections of these proxies from diagenetic overprint have been proposed (e.g., Schrag et al., 1995; Rosenthal and Lohmann, 2002), only a few studies exist on the diagenetic effects of organic matter decomposition on bulk parameters used for paleoenvironmental studies. The importance of TOC corrections for petroleum studies is well known and several corrections specific to source rocks are available but they have not been applied to paleoenvironmental reconstructions until recently (Hart and Hofmann, 2022). In a marine core from the Timor Sea, Gupta and Kawahata (2006) observed a high impact of diagenesis on labile components (amino acids) and proposed a correction of the measured total organic carbon (TOC) using a linear equation. They suggest that corrected organic carbon more accurately reflects the original organic carbon deposited on the sea floor and thus is more appropriate for primary productivity estimates. In this paper, we focus on bulk organic data from a peatcore situated on the Adamawa Plateau in Cameroon. Several maar lakes from the Adamawa Plateau have been studied for paleoclimatic and paleoenvironmental reconstruction (e.g., Ngos III et al., 2003; Vincens et al., 2010; Nguetsop et al., 2011; Lebamba et al., 2016; N'nanga et al., 2021) but until now no peat deposit has been investigated. We propose a method to deconvoluate the diagenetic signal from the climatic signal in peat. We develop a model that allows subtraction of a mean decomposition signal from bulk parameters such as TOC, $\delta^{13}C$ and C/N. Residual data provide a robust means of interpreting palaeoclimatic and palaeoenvironmental variations in parameters for which the decomposition signal is the main mode of variability (in particular TOC).

1. Study site and materials

1.1. Study site

The NGaoundaba peat deposit (N7.13542° E13.69009°, 1175m above sea level) is located in North Cameroon near the city of NGaoundéré on the Adamawa Plateau, occupying a volcanic crater situated next to Lake Tabéré. Its current surface area covers ~18 000 m^2, and the maximum depth is still unknown. According to Letouzey (1958), the peat deposit is situated in the soudano-guinean shrubs savannas from the Adamawa Plateau. Nowadays, the peat is covered by sedges (Cyperaceae), that are annually burned. Tropical peatlands of Africa from similar settings are largely sedge-dominated and peat composition is a mix of sedges and woody remains from the surrounding forests (Dargie, 2015).

1.2. Sampling

A 6-meter-long core was collected on February 2019 using a Russian peat corer. The core is composed of twelve consecutive 50-cm sections and consists of dark brown peat containing plant debris. The color is consistently dark brown over the whole core. The NGaoundaba peat deposit is continuous and essentially composed of peat without sandy or clayey zones. The core was subsampled at 2.5-cm intervals corresponding to a resolution of around 40yr. Samples were freeze-dried prior to analysis.

2. Analytical methods

2.1. Dating

The chronological framework of NGaoundaba sequence is based on 30 radiocarbon dates carried out at the LMC14 Laboratory (Saclay, France) following the procedure from Dumoulin et al. (2017) and Moreau et al. (2013). Measurements were performed on bulk peat sediment. Data were compiled

using the R-software Bacon v2.5 (Blaauw and Christen, 2011) and calibrated using the SHCal20 calibration curve (Hogg et al., 2020) and postbomb calibration curve NH3 (Hua et al., 2013).

2.2. Rock-Eval® thermal analysis

Rock-Eval® analyses were performed on 69 samples using 10 mg of ground peat and a Rock-Eval® 6 (Vinci Technologies, France). The Rock-Eval® thermal analysis is based on continuous measurement of effluents, i.e., hydrocarbons (HC), carbon monoxide (CO), and carbon dioxide (CO_2), released during the thermal cracking of organic compounds under pyrolytic conditions (from 200 to 650°C at 25°C min^{-1} in an inert atmosphere), followed by the combustion of residual organic compounds (from 200 to 850°C in an oxidative atmosphere). The resulting thermograms were used to calculate the standard parameters by integrating the amounts of HC, CO, and CO_2 within the defined temperature limits (Lafargue et al., 1998; Behar et al., 2001). The Total Organic Carbon (TOC parameter) is calculated as the sum of all C effluents (i.e., HC, CO, and CO_2) under a temperature limit (Lafargue et al., 1998) and usually represents the amount of organic C. When inorganic carbon forms are negligible, the percent C is calculated as the sum of organic carbon (TOC) and MinC parameter. The Hydrogen Index (HI) corresponds to the amount of HC released during pyrolysis relative to percent C. In organic samples with the same source of organic inputs, a decrease in HI is usually related to the decomposition of H-rich organic compounds (dehydrogenation), leading to an enrichment of aromatic compounds during diagenesis in lake deposits (Meyers and Lallier-Vergès, 1999) or pedogenesis in soils (Disnar et al., 2003; Barré et al., 2016). In addition to the above standard parameters, Disnar et al. (2003) proposed using the shape of thermograms to obtain additional information about OM quality. In the present study, we used the I index to quantify the preservation of the thermolabile C pool (Sebag et al., 2016). This index is derived from the integrated S2 areas in specific temperature ranges (200--400 °C, 400--460 °C, and > 460 °C), and is usually interpreted in terms of specific thresholds of the thermal stability of organic compounds, separating the thermolabile, thermoresistant, and thermorefractory C pools (Disnar et al., 2003; Sebag et al., 2006; Saenger et al., 2013). The I-index has recently been used to measure the degree of decomposition of a tropical peat to identify an event of increased decomposition of organic matter after deposit (Garcin et al., 2022).

While it is well calibrated for sedimentary organic matter (i.e., kerogens), Rock-Eval® percent C needs to be corrected in soils and litters (Disnar et al., 2003). The correction factor calculation depends on an estimation of the decomposition state of the sediment. As decomposition state is a focus of this study, we chose to use elemental and stable isotope analyses rather than Rock-Eval® analyses for data processing to avoid the use of any pre-processing assumption of decomposition state.

2.3. Elemental and stable isotope analyses

A total of 66 samples was ground and homogenized, then measured for TOC, total nitrogen, and $\delta^{13}C$ composition of TOC. Between 2 and 4 mg of non-acidified sediment were combusted in tin capsules using an elemental analyser (Vario Micro Cube Elementar) coupled to a thermal conductivity detector and an isotope ratio mass spectrometer IRMS (Elementar Vision). The carrier gas was helium. Samples were first passed through a combustion furnace at 950°C under an excess of oxygen with copper oxide as an oxidation catalyst, producing CO_2, N_xO_x, and H_2O. Then, a reduction furnace at 550°C reduced N_xO_x to N_2 and removed excess O_2 using reduced copper. H_2O was trapped and removed using a phosphorous pentoxide chemical trap. N_2 and CO_2 were separated using a purge and trap desorption column. The C/N ratio was calculated as the ratio between TOC and wt%N.

A working standard (IVA sediment) was analysed every 10 samples and used to normalize the mass spectrometer signals. Triplicates were analysed every 3 samples and standard deviations were calculated. The absence of carbonates in the samples was confirmed by acid-treating 6 samples (1 every meter) using vapour of 12N hydrochloric acid for 72 hours and then performing a comparative analysis.

3. Data processing

3.1. General information

The method proposed in this study is divided into 4 steps (Fig. 2) and described in detail below. Kinetics of organic compound degradation follow a simple first order equation (Westrich and Berner, 1984; Grossi et al., 2003) with different reactivity depending on the compounds. The increase in the proportion of recalcitrant compounds leads to a progressive increase in carbon concentration despite the total mass loss (Fig. 1). Using a different approach, Clymo (1984) and Clymo et al. (1998) developed models of peat accumulation. Based on equation 1, α denotes the manner of decay and constant, linear and quadratic rules were tested by Clymo et al. (1998). Using a linear decay rule α_L*, the plot of peat growth (cumulative carbon M_t) follows the logarithmic equation (2) with p* the rate of addition of dry mass at the top of the peat deposit (Clymo et al., 1998).

$$\frac{d\mu}{dt} = -\alpha \times \mu \; with \; \mu = \frac{m_t}{m_0} \qquad (1)$$

$$M_t = \frac{p^*}{\alpha_L^*} \times \ln(1 + \alpha_L^* \times t) \qquad (2)$$

Based on these observations and on the logarithmic trend followed by TOC with age and depth in our dataset and in several others (e.g., Upton et al., 2018; Wei et al., 2012; Garcin et al., 2022), we chose to use a natural logarithmic function (noted "ln") in two possible forms presented in equations 3 and 4 using age as the variable. The parameter c can be linked to the initial C content in freshly deposited organic matter, while a and b are related to the kinetic constants and the proportion of labile versus recalcitrant organic matter.

$$f(x) = a \times \ln(b \times t) + c \quad \forall t \in \Re^{+*} \qquad (3)$$

$$f(x) = a \times \ln(b \times t + d) + c \quad \forall t \in \;]-d/b, +\infty[. \qquad (4)$$

Data processing was performed using the Python software. The different parameters a, b, c and d of each function are optimized using the curve.fit() function of the SciPy Python library. The difference between the two forms is slight; equation 4 allows an offset on the t axis of the data and the domains of the function defined as the set of *t*-values accepted by the function are slightly different for the two functions. By definition, the ln function is only defined for strictly positive values, equation 3 is defined for strictly positive values $\Re^{+*}$, while equation 4 is defined for t above the ratio of d and b parameters -d/b (i.e. for $t \in$]-d/b; +∞[).

The choice of the function for each parameter was determined by comparing the determination coefficient r^2 between the raw data and the curve-fit for each form. We called "raw data" the initial data prior to any data treatment.

3.2. Data normalization

As logarithmic functions can only be used for positive and non-zero values, raw data were normalized (scaling of all values in the range of 0 and 1) prior to any analysis (Fig. 2 - Step1). Practically, all values

were normalized using the MinMaxscaler transforms from Python library sklearn.preprocessing based on the following equation 5:

$$x_{scaled} = \frac{x - x_{min}}{x_{max} - x_{min}} \qquad (5)$$

We add 0.001 to all normalized ages to avoid having a zero *t*-value that cannot be used in a logarithmic function.

3.3. Total curve fitting and derivative calculation

The method is based on two successive curve fittings, which are presented in the next two subsections. The objective is to find a curve fit based only on a part of the initial dataset where the decomposition is predominant.

A first option would use the upper oxic layer thickness (acrotelm) as most of the decomposition occurs in this layer (Clymo, 1984). However, no measurement of this parameter is available for the NGaoundaba peat deposit. Based on the mean water table depth, upper oxic layer thicknesses between 5 and 35 cm were estimated for several temperate peat deposits (Kuhry and Vitt, 1996; Evans et al., 1999; Weijers et al., 2004, 2006; Liu et al., 2010; Drollinger et al., 2019). In a tropical peat swamp forest, Jauhiainen et al. (2005) reported a water table varying between 80 cm under and 20 cm above the peat sediment surface throughout the year with maximum occurrences of values between 10 and 30 cm under the peat sediment surface. The upper oxic layer thickness is usually on the order of tens of centimeters. In the case of the NGaoundaba dataset, neither measurement of the upper layer thickness nor estimation based on literature can be used for the modeling as it would involve only a few points and would lead to poorly constrained results.

To determine the age where the decomposition is the main parameter controlling bulk organic data, we first fit the logarithmic function *f* using all x-values, then we calculate the derivative of this function *f'* and determine the range of x-values where *f'*(x)>1, thus finding the inflection point of the curve (Fig.2 - Step 2 and Fig.3 - Light colored curves). The value *f'*(x)>1 was fixed arbitrarily. This choice avoids using the whole dataset for the modeling and avoids purely circular reasoning.

3.4. Partial curve fitting

A new function *g* is then fitted based only on the reduced range of x-values (Fig. 2 - Step 3 and Fig. 3). In other words, only a part of the original data is selected for the final curve fitting *g*. For each parameter, the selected x-values are indicated in dark color on Figure 3. A total of 13, 17 and 11 x-values were selected for TOC, $\delta^{13}C_{bulk}$ and C/N, respectively.

3.5. Curve fit subtraction

The last step is the subtraction of the function *g* (i.e., the modeled data) to the raw data. The resulting data are named the residual data. Thus, positive residual values indicate that the raw data values are superior to those of the modeled data, indicating an excess of this parameter compared to the modeled data. Residual data are smoothed (Fig. 2 - Step 4) using a moving average method.

4. Results

4.1. Age model

Calibrated ages range from -39 a cal BP at 10 cm depth to 9642 a cal BP at the bottom (590 cm) (Fig. 4, Tab. 1). The age-depth model presents a quite uniform sediment accumulation rate except around 150 cm-depth (2.5 ka cal BP) and 200 cm-depth (4.0 ka cal BP). These two periods are not situated at the limit between two core sections, as indicated on figure 4.

4.2. Elemental raw data

TOC increases with increasing depth and age ranging from 26.76 to 53.5 % for elemental and stable isotope analyses (Fig. 5(A)).

The C/N ratio roughly increases with depth and age. Until 4.5 ka cal BP, values increase nearly linearly (Fig. 5(C)). From 4.5 to around 5 ka cal BP, the C/N ratio decreases and then stabilizes until 7.1 ka cal BP. The bottom of the core is marked by a general increase of the C/N ratio with small-scale variations. The range of values of elemental raw data is consistent with data reported for other African peat deposits (e.g., Aucour et al., 1999; Baker et al., 2014; Strobel et al., 2019).

4.3. Rock-Eval® I-index and HI

The I-index ranges from 0.06 to 0.37. The I-index variations can be divided into two periods (Fig. 5(D)). The first period from the present to 6.4 ka cal BP is characterized by a regular decrease in I-index from 0.37 to 0.08. The second period from 6.4 ka cal BP to the bottom of the core presents more variations, but with a narrower amplitude between 0.2 and 0.06 (Fig. 5(D)).

The HI ranges from 195 to 427 (Fig. 6(G)). The HI is between 250 and 300 from 5.8 ka cal BP until present except between 4 and 3 ka cal BP where values are around 225. The highest HI values are found from 7.9 to 5.8 ka cal BP and at the bottom of the core. From 9.4 to 7.9 ka cal BP, HI values are under 300 (Fig. 6(G)).

4.4. Isotopic raw data

The $\delta^{13}C_{bulk}$ presents a general decrease with increasing depth and age ranging from -15.6 to -26.3‰ (Fig. 5(B)). The $\delta^{13}C_{bulk}$ decreases from the top of the core to 3 ka cal BP from values around -16‰ to values around -22‰. Between 3 and 4 ka cal BP, $\delta^{13}C_{bulk}$ is close to -25‰. The $\delta^{13}C_{bulk}$ increases between 4 ka cal BP and 5.8 ka with most values between -23 and -20.4‰ compared to values around –25 between 5.8 and 9.4 ka cal BP. The $\delta^{13}C_{bulk}$ also increases from 9.4 ka to the bottom of the core ranging from -21.4 to -20.4 ‰ during this period.

4.5. Processed residual data

Processed residual data range from -0.126 to 0.181, -0.189 to 0.815 and -0.090 to 0.782 for TOC, $\delta^{13}C_{bulk}$ and C/N respectively. Both residual TOC, residual $\delta^{13}C_{bulk}$ and residual C/N are mostly positive (Fig. 6(C), (D) and (E) respectively).

Residual TOC values are decreasing from the bottom of the core until 8 ka cal BP with values close zero between 9 and 8 ka cal BP (Fig. 6(D)). From 8 to 4 ka cal BP, residual TOC are between 0.1 and 0.2 except around 5.5 ka cal BP where values are slightly lower. From 2.5 ka cal BP until present, TOC values present rapid variations between -0.13 and 0.12.

The residual $\delta^{13}C_{bulk}$ presents a general decreasing trend and positive values from the bottom of the core to around 4 ka cal BP (Fig. 6(E)). The period of less depleted values from 5.8 to around 4 ka cal BP observed in the raw $\delta^{13}C_{bulk}$ data (Fig. 5(B)) is still visible in the residual $\delta^{13}C_{bulk}$ with positive residual data ranging from 0.2 to 0.5.

The residual C/N presents similar variations as the raw C/N data with a globally increasing trend with depth and age (Fig. 6(F)). Values are close to zero until 2.5 ka cal BP and between 5 and 7.5 ka cal BP. The highest values occur between 8.5 and 9 ka cal BP.

5. Discussion

5.1. Interpreting the residual data

The log-generated data represent the part of the signal due to decomposition. Residual values close to 0 indicate a good correspondence between the original data and the log-generated data (Fig. 6). Higher values (both positively and negatively) indicate a greater difference between raw data and the model and suggest either a change in the decomposition compared to the model or the influence of other parameters that will be discussed in the next paragraphs.

In a simple approach, the carbon accumulation in peatlands can be described as a balance between vegetation inputs and decomposition (Frolking et al., 2001; Kurnianto et al., 2015). Even if microbial organic matter is generally not considered in the mass balance, microbial activity is a key point of decomposition processes (Moore, 1989). The TOC excess is thus linked to either reduced decomposition or an increase in deposition compared to the mean decomposition signal (and vice-versa). Changes in paleo -climate and -environment exert a strong influence on these parameters.

5.2. Influence of water table depth

An increase in wetness leads to changes in peatland surface structure and an increase in carbon sequestration by increasing litter production and decreasing litter decay losses (Belyea and Malmer, 2004). These changes are driven by an increase in acrotelm thickness due to a rise of the water table (Belyea and Malmer, 2004). Moisture content, redox potential and pH control the microbial community structure and can limit or enhance the presence of key decomposers (Girkin et al., 2020), even in deep peat deposits (Kluber et al., 2020). Furthermore, Ise et al. (2008) demonstrate the existence of a positive feedback between accumulation of soil organic carbon, water table depth and decomposition rates, highlighting the high sensitivity of peatland to climate variations. Hodgkins et al. (2018) demonstrated that the recalcitrance of tropical peat deposits is higher than that of boreal peat deposits which allows them to persist despite warmer and sometimes drier conditions. Tropical peat also accumulates because of the low decomposition of roots and woods under anoxic conditions when the water table is high (Chimner and Ewel, 2005).

The positive values of residual TOC before ca 4 ka cal BP (Fig. 6(D)) could indicate a period of increased wetness leading to a rise of the water table favouring preservation of the organic matter. This period is consistent with the timing of the African Humid Period (AHP), beginning around 14.5 ka cal BP and

ending between 6 and 4 ka cal BP (among others, Demenocal et al., 2000; Kröpelin et al., 2008; Amaral et al., 2013). The period between 9 and 8 ka cal BP that presents residual TOC close to zero could correspond to a relatively drier intermission during the AHP.

5.3. Influence of changes in vegetation

Major shifts in vegetation also have a strong influence on both decomposition and deposition of organic matter (Belyea and Malmer, 2004). Tropical peat deposits may be visually uniform despite considerable changes in vegetation inputs (Page et al., 1999). The visual homogeneity of the NGaoundaba peat deposit does not exclude changes in the vegetation. A reciprocal relation between carbon storage and plant species diversity has been identified in a tropical peat deposit from Sumatra (Shimamura and Momose, 2007). Changes in the sources of organic matter have an influence on the initial proportion of thermo-labile vs thermo-stable organic matter (Wang et al., 2015) and, thus, on the evolution of this organic matter during decomposition. Major changes in vegetation are reported at the end of the African humid period (AHP) (Maley and Brenac, 1998; Vincens et al., 2010) and could explain part of the observed variations in residual TOC by changing the type and amount of vegetation inputs to the peatland.

To identify the period where the signal is most influenced by vegetation changes at the NGaoundaba peat deposit, we use $\delta^{13}C_{bulk}$, both raw and residual (Fig. 5(B) and fig. 6(E)). Skrzypek et al. (2010) demonstrated that the primary $\delta^{13}C$ signal of peat-forming plants is preserved and that decomposition has only a secondary influence on the $\delta^{13}C_{bulk}$ signal. The latter has been directly used to describe changes in C3/C4 vegetation (Baker et al., 2014).

The two main periods observed in the residual $\delta^{13}C_{bulk}$ data before and after around 4 ka cal BP are roughly consistent with the timing of the AHP (Fig. 6(E)). The raw $\delta^{13}C_{bulk}$ values close to -25‰ until 5.8 ka cal BP are consistent with a C3-dominated environment suggesting predominance of forest taxa (Fig. 5(B)). The period from 5.8 to around 4 ka cal BP highlighted in both residual and raw $\delta^{13}C_{bulk}$ presents less depleted values. It may suggest a short transition to C4-dominated savanna taxa followed by a short return of the C3-dominated environment between 4 and 3 ka cal BP, with raw $\delta^{13}C_{bulk}$ around -25‰. After 3 ka cal BP, the signal is consistent with an increasing influence of C4-type plants.

Human activities such as turning peatland into cultured field also can have an impact on the accumulation of carbon (Wang et al., 2017) and, consequently, on the $\delta^{13}C_{bulk}$ signature (Lane et al., 2008). The influence of human occupation on sedimentary archives is reported in several studies from West Africa during late Holocene such as around 2.6 ka cal BP at lake Barombi MBo (Cameroon) (Garcin et al., 2018) or after 2.2 ka cal BP in the Congo River Basin (Bayon et al., 2019). It cannot be excluded that the recent history of the NGaoundaba peat deposit was influenced by human occupation.

5.4. Influence of C-cycling and microbial organic matter

Peat deposits can shift from a sink to a source of CO_2 and CH_4 gases reflecting changes in the microbial communities and associated biogeochemical processes such as methanotrophy and methanogenesis (Jauhiainen et al., 2005; Roehm, 2005). Even if the proportion, in terms of the mass of the microbial organic matter, is not large, the specific $\delta^{13}C$ signature of some microbial compounds may not be negligible. Indeed, some carbon sources such as methane can present important variations of their

carbon isotopic composition and values as depleted as -110‰ for direct reduction of CO_2 to CH_4 (Whiticar, 1999). The $\delta^{13}C$ of methanotrophs' biomass is generally close to the carbon source signature even if depletion or enrichment of cellular components can be observed depending on metabolic pathway or environmental parameters (Jahnke et al., 1999). Thus, even a small proportion of highly ^{13}C-depleted microbial biomass could significantly modify the $\delta^{13}C_{bulk}$.

Mosses such as Sphagnum spp. can use recycled carbon in wet environments (Price et al., 1997; Nichols et al., 2009). By extension, $\delta^{13}C_{bulk}$ has also been proposed to reflect variations in the uptake of C recycled from methanogenesis with enriched values corresponding to periods of high methanogenesis (Jones et al., 2010). However, Sphagnum are not present at the NGaoundaba peatland, which is dominated by sedges, so $\delta^{13}C_{bulk}$ cannot be interpreted this way. As an example, if we consider CH_4 with a $\delta^{13}C$ signature close to -60‰, taking into account both direct reduction of CO_2 to CH_4 and acetotrophic methanogenesis (Whiticar, 1999). In a first approximation, we can consider that bulk organic matter produced by consumption of this methane will have a similar $\delta^{13}C$ signature as the source CH_4. Even a 1% input of this microbial organic matter in the bulk will lead to a decrease of more than 0.5‰ of the $\delta^{13}C_{bulk}$. Present bulk data don't give us much information about microbial activity. However, it is important to keep in mind that a microbial signal can superimpose on the primary $\delta^{13}C_{bulk}$ signal and either increase or mask pre-existing variations. Kuhry and Vitt (1996) compared the evolution of bulk C/N in both the acrotelm and catotelm in a Sphagnum peat, suggesting a predominant impact of peat decomposition on C/N values. The increase in acrotelm is interpreted as a preferential N loss in oxic conditions while the decrease in catotelm is consistent with a predominance of methanogenesis affecting C content while N is no longer affected by decomposition and is much less mobile in the sediment under anoxic conditions. These observations are not consistent with the general increase observed in C/N in the NGaoundaba peat deposit (Fig. 6(G)). This increase follows the general increase observed in TOC and is interrupted by a short interval from 9 to 8 ka cal BP when the C/N increases and might suggest a change in the origin of the organic matter (Talbot and Johannessen, 1992).

5.5. Validation and limits of the approach

The decreasing I-index observed in the NGaoundaba peat deposit from 6.4 ka cal BP to the surface reflects the decrease of thermolabile compounds and the relative increase in thermostable compounds, reflecting the progressive decomposition of labile organic matter and the increase in thermal stability of organic matter from 6.4 ka cal BP until present (Sebag et al., 2016) (Fig. 5(D)). During this period, raw TOC increases, indicating an enrichment in thermostable C-rich compounds relatively to thermolabile compounds more rich in heteroatoms. Between the bottom of the core and 6.4 ka cal BP, the I-index remains rather stable; it is likely that most thermolabile compounds are decomposed and it is consistent with a raw TOC around 50% with limited variations during this period.

Our method is based on the observation that for this particular peat deposit, the TOC increases progressively with depth and follows nearly exactly a logarithmic curve. The function used for the modelling will depend on the dynamics of the system (Clymo et al., 1998). Thus, this method is undoubtedly not applicable to all peat deposits. This increasing trend is expected for peats composed almost entirely of organic matter. The presence of mineral-rich intervals such as clayey or sandy intervals or a steady input of a large amount of mineral matter will affect this trend (Baker et al., 2014; Njagi et al., 2021). Such records are therefore not ideal for the modeling presented in this study. The method gives a lot of weight to the top values of the core and slight analytical errors in these values could have a strong impact on the model.

As vegetation may be the primary factor controlling $\delta^{13}C_{bulk}$ (Skrzypek et al., 2010), the curve fitting might be distorted by the primary impact of vegetation changes. It may explain why the curve fitting for $\delta^{13}C$ is not as good as for TOC with the modeling function rapidly diverging from the data (Fig. 3). The residual $\delta^{13}C_{bulk}$ (Fig. 6(E)) erases two periods of relatively enriched $\delta^{13}C_{bulk}$ from 5.8 to 4 ka cal BP and from the bottom of the core to 9 ka cal BP visible in the raw $\delta^{13}C_{bulk}$ record (Fig. 5(B)).

The comparison between residual TOC and HI from the same peatcore shows striking similarities (Fig. 6(D) & (G)). The HI can be controlled by the degree of decomposition but can also reflect changes in the origin of the organic matter (Sebag et al., 2016). The higher values observed between 8 and 6 ka cal BP and at the bottom of the core tend to indicate well preserved terrestrial organic matter that is consistent with the TOC data and the wettest period of the African Humid Period. The decrease in HI between 9 and 8 ka cal BP suggests a change in the origin of the organic matter or in its decomposition and is consistent with the increase in the C/N ratio observed at the same period.

Conclusions

The present case study based on a West-African peat deposit presents several interesting characteristics: it is nearly continuous, macroscopically homogeneous without clayey passages, and some bulk parameters such as TOC present a strong logarithmic trend with age. Thus, it is possible to propose a method to isolate and subtract the part of the variation only due to the decomposition of organic matter and interpret the residual variations as modifications of the environmental conditions. The residual TOC obtained with our method highlights well-known climatic transitions and variations such as the African Humid Period and presents similar variations as other parameters such as HI. Results obtained from residual C/N and $\delta^{13}C_{bulk}$ are more questionable, suggesting a greater impact of parameters other than decomposition on the variations, such as vegetation shifts (Skrzypek et al., 2010; Baker et al., 2014), changes in microbial processes (Moore, 1989; Girkin et al., 2020) or detrital input (Amorim et al., 2022) associated with differences in the way the decomposition processes affect these parameters (Ågren et al., 1996). Based only on bulk organic parameters, it is difficult to precisely constrain the origin and timing of the proposed environmental and climatic changes, thus the use of other proxies such as pollen data and biomarkers will help to confirm or infirm the climatic and environmental interpretation proposed here.

This method is certainly not applicable to all peat deposits and we recommend a careful analysis of the data and testing before applying it. We recommend applying this method to records composed almost entirely of organic matter and without significant variation in the mineral fraction. This method is a quick and straightforward way to obtain a first overview of the paleoclimatic and paleoenvironmental variations from a new sediment core based on bulk analytical methods (Elemental Analysis and Rock-Eval®). It can help to identify periods of great interest for more intensive investigations (e.g., pollen, biomarkers), by highlighting the main transitions visible in bulk organic data.

Acknowledgements

This study was supported by the ANR project TAPIOCA (ANR-18-CE01-0005) granted to G.Ménot and by a PhD scholarship from the ENS de Lyon to V.Schaaff. Radiocarbon dating has been supported through the French CNRS-INSU-IRD Radiocarbon program and performed at the LMC14 laboratory

with the ARTEMIS faciliy in Saclay. Rock-Eval® is a trademark registered by IFP Energies Nouvelles. We thank P. Meyers and C.C. Walters for constructive comments on an earlier draft of the manuscript.

References

Ågren, G.I., Bosatta, E., Balesdent, J., 1996. Isotope discrimination during decomposition of organic matter: a theoretical analysis. Soil Science Society of America Journal 60, 1121–1126.

Amaral, P., Vincens, A., Guiot, J., Buchet, G., Deschamps, P., Doumnang, J.-C., Sylvestre, F., 2013. Palynological evidence for gradual vegetation and climate changes during the African Humid Period termination at 13 N from a Mega-Lake Chad sedimentary sequence. Climate of the Past 9, 223–241.

Amorim, H.C., Hurtarte, L.C., Souza, I.F., Zinn, Y.L., 2022. C: N ratios of bulk soils and particle-size fractions: Global trends and major drivers. Geoderma 425, 116026.

Aucour, A.-M., Bonnefille, R., Hillaire-Marcel, C., 1999. Sources and accumulation rates of organic carbon in an equatorial peat bog (Burundi, East Africa) during the Holocene: carbon isotope constraints. Palaeogeography, Palaeoclimatology, Palaeoecology 150, 179–189.

Aucour, A.-M., Hillaire-Marcel, C., Bonnefille, R., 1996. Oxygen isotopes in cellulose from modern and quaternary intertropical peatbogs: implications for palaeohydrology. Chemical Geology 129, 341–359.

Baker, A., Routh, J., Blaauw, M., Roychoudhury, A., 2014. Geochemical records of palaeoenvironmental controls on peat forming processes in the Mfabeni peatland, Kwazulu Natal, South Africa since the Late Pleistocene. Palaeogeography, Palaeoclimatology, Palaeoecology 395, 95–106.

Barré, P., Plante, A.F., Cécillon, L., Lutfalla, S., Baudin, F., Bernard, S., Christensen, B.T., Eglin, T., Fernandez, J.M., Houot, S., Kätterer, T., Le Guillou, C., Macdonald, A., van Oort, F., Chenu, C., 2016. The energetic and chemical signatures of persistent soil organic matter. Biogeochemistry 130, 1–12.

Bayon, G., Schefuß, E., Dupont, L., Borges, A.V., Dennielou, B., Lambert, T., Mollenhauer, G., Monin, L., Ponzevera, E., Skonieczny, C., André, L., 2019. The roles of climate and human land-use in the late Holocene rainforest crisis of Central Africa. Earth and Planetary Science Letters 505, 30–41.

Behar, F., Beaumont, V., De B. Penteado, H.L., 2001. Rock-Eval 6 technology: performances and developments. Oil & Gas Science and Technology 56, 111–134.

Behling, H., Safford, H.D., 2010. Late-glacial and Holocene vegetation, climate and fire dynamics in the Serra dos Órgãos, Rio de Janeiro State, southeastern Brazil. Global Change Biology 16, 1661–1671.

Belyea, L.R., Malmer, N., 2004. Carbon sequestration in peatland: patterns and mechanisms of response to climate change. Global Change Biology 10, 1043–1052.

Benner, R., Fogel, M.L., Sprague, E.K., Hodson, R.E., 1987. Depletion of ^{13}C in lignin and its implications for stable carbon isotope studies. Nature 329, 708–710.

Berger, A., Guiot, J., Kukla, G., Pestiaux, P., 1981. Long-term variations of monthly insolation as related to climatic changes. Geologische Rundschau 70, 748–758.

Berner, R.A., 2020. Early diagenesis. Princeton University Press.

Biester, H., Knorr, K.-H., Schellekens, J., Basler, A., Hermanns, Y.-M., 2014. Comparison of different methods to determine the degree of peat decomposition in peat bogs. Biogeosciences 11, 2691–2707.

Blaauw, M., Christen, J.A., 2011. Flexible paleoclimate age-depth models using an autoregressive gamma process. Bayesian analysis 6, 457–474.

Bonnefille, R., Riollet, G., Buchet, G., Icole, M., Lafont, R., Arnold, M., Jolly, D., 1995. Glacialanterglacial record from intertropical Africa, high resolution pollen and carbon data at Rusaka, Burundi. Quaternary Science Reviews 14, 917–936.

Booth, R.K., Jackson, S.T., Gray, C.E., 2004. Paleoecology and high-resolution paleohydrology of a kettle peatland in upper Michigan. Quaternary Research 61, 1–13.

Chambers, F.M., Beilman, D.W., Yu, Z., 2011. Methods for determining peat humification and for quantifying peat bulk density, organic matter and carbon content for palaeostudies of climate and peatland carbon dynamics. Mires and Peat 7, 1–10.

Chimner, R.A., Ewel, K.C., 2005. A tropical freshwater wetland: II. Production, decomposition, and peat formation. Wetlands Ecology and Management 13, 671–684.

Clymo, R.S., 1984. The limits to peat bog growth. Philosophical Transactions of the Royal Society of London. B, Biological Sciences 303, 605–654.

Clymo, R.S., Turunen, J., Tolonen, K., 1998. Carbon accumulation in peatland. Oikos 368–388.

Cooper, H.V., Vane, C.H., Evers, S., Aplin, P., Girkin, N.T., Sjögersten, S., 2019. From peat swamp forest to oil palm plantations: The stability of tropical peatland carbon. Geoderma 342, 109–117.

Dargie, G.C., 2015. Quantifying and understanding the tropical peatlands of the central Congo basin (PhD Thesis). University of Leeds.

Demenocal, P., Ortiz, J., Guilderson, T., Adkins, J., Sarnthein, M., Baker, L., Yarusinsky, M., 2000. Abrupt onset and termination of the African Humid Period: rapid climate responses to gradual insolation forcing. Quaternary science reviews 19, 347–361.

Diefendorf, A.F., Freimuth, E.J., 2017. Extracting the most from terrestrial plant-derived n-alkyl lipids and their carbon isotopes from the sedimentary record: A review. Organic Geochemistry 103, 1–21.

Disnar, J.-R., Guillet, B., Kéravis, D., Di-Giovanni, C., Sebag, D., 2003. Soil organic matter (SOM) characterization by Rock-Eval pyrolysis: scope and limitations. Organic geochemistry 34, 327–343.

Dodla, S.K., Wang, J.J., DeLaune, R.D., 2012. Characterization of labile organic carbon in coastal wetland soils of the Mississippi River deltaic plain: relationships to carbon functionalities. Science of the total environment 435, 151–158.

Drollinger, S., Kuzyakov, Y., Glatzel, S., 2019. Effects of peat decomposition on ^{13}C and ^{15}N depth profiles of Alpine bogs. Catena 178, 1–10.

Dumoulin, J., Comby-Zerbino, C., Delqué-Količ, E., Moreau, C., Caffy, I., Hain, S., Perron, M., Thellier, B., Setti, V., Berthier, B., Beck, L., 2017. Status report on sample preparation protocols developed at the LMC14 Laboratory, Saclay, France: from sample collection to 14C AMS measurement. Radiocarbon 59, 713–726.

Evans, M.G., Burt, T.P., Holden, J., Adamson, J.K., 1999. Runoff generation and water table fluctuations in blanket peat: evidence from UK data spanning the dry summer of 1995. Journal of

574 Hydrology 221, 141–160.

575 Frolking, S., Roulet, N.T., Moore, T.R., Richard, P.J., Lavoie, M., Muller, S.D., 2001. Modeling
576 northern peatland decomposition and peat accumulation. Ecosystems 4, 479–498.

577 Garcin, Y., Deschamps, P., Ménot, G., De Saulieu, G., Schefuß, E., Sebag, D., Dupont, L.M., Oslisly,
578 R., Brademann, B., Mbusnum, K.G., Onana, J.-M., Ako, A.A., Epp, L.S., Tjallingii, R., Strecker,
579 M.R., Brauer, A., Sachse, D., 2018. Early anthropogenic impact on Western Central African
580 rainforests 2,600 y ago. Proceedings of the National Academy of Sciences 115, 3261–3266.

581 Garcin, Y., Schefuß, E., Dargie, G.C., Hawthorne, D., Lawson, I.T., Sebag, D., Biddulph, G.E.,
582 Crezee, B., Bocko, Y.E., Ifo, S.A., Mampouya Wenina, Y.E., Mbemba, M., Ewango, C.E.N., Emba,
583 O., Bola, P., Kanyama Tabu, J., Tyrrell, G., Young, D.M., Gassier, G., Girkin, N.T., Vane, C.H.,
584 Adatte, T., Baird, A.J., Boom, A., Gulliver, P., Morris, P.J., Page, S.E., Sjögersten, S., Lewis, S.L.,
585 2022. Hydroclimatic vulnerability of peat carbon in the central Congo Basin. Nature 1–6.

586 Girkin, N.T., Lopes dos Santos, R.A., Vane, C., Ostle, N., Turner, B.L., Sjögersten, S., 2020. Peat
587 properties, dominant vegetation type and microbial community structure in a tropical peatland.
588 Wetlands 40, 1367–1377.

589 Grossi, V., Caradec, S., Gilbert, F., 2003. Burial and reactivity of sedimentary microalgal lipids in
590 bioturbated Mediterranean coastal sediments. Marine Chemistry 81, 57–69.

591 Gupta, L.P., Kawahata, H., 2006. Downcore diagenetic changes in organic matter and implications for
592 paleoproductivity estimates. Global and Planetary Change 53, 122–136.

593 Hart, B.S., Hofmann, M.H., 2022. Revisiting paleoenvironmental analyses and interpretations of
594 organic-rich deposits: The importance of TOC corrections. Organic Geochemistry 170, 104434.

595 Hodgkins, S.B., Richardson, C.J., Dommain, R., Wang, H., Glaser, P.H., Verbeke, B., Winkler, B.R.,
596 Cobb, A.R., Rich, V.I., Missilmani, M., Flanagan, N., Ho, M., Hoyt, A.M., Harvey, C.F., Vining,
597 S.R., Hough, M.A., Moore, T.R., Richard, P.J.H., De La Cruz, F.B., Toufaily, J., Hamdan, R.,
598 Cooper, W.T., Chanton, J.P., 2018. Tropical peatland carbon storage linked to global latitudinal trends
599 in peat recalcitrance. Nature Communications 9, 3640.

600 Hogg, A.G., Heaton, T.J., Hua, Q., Palmer, J.G., Turney, C.S., Southon, J., Bayliss, A., Blackwell,
601 P.G., Boswijk, G., Bronk Ramsey, C., Pearson, C., Petchey, F., Reimer, P., Reimer, R., Wacker, L.,
602 2020. SHCal20 Southern Hemisphere calibration, 0–55,000 years cal BP. Radiocarbon 62, 759–778.

603 Hua, Q., Barbetti, M., Rakowski, A.Z., 2013. Atmospheric radiocarbon for the period 1950–2010.
604 Radiocarbon 55, 2059–2072.

605 Inglis, G.N., Naafs, B.D.A., Zheng, Y., Schellekens, J., Pancost, R.D., "the T-GRES peat database
606 collaborators," 2019. ^{13}C values of bacterial hopanoids and leaf waxes as tracers for methanotrophy in
607 peatlands. Geochimica et Cosmochimica Acta 260, 244–256.

608 Ingram, H., 1978. Soil layers in mires: function and terminology. Journal of Soil Science 29, 224–
609 227.

610 Ise, T., Dunn, A.L., Wofsy, S.C., Moorcroft, P.R., 2008. High sensitivity of peat decomposition to
611 climate change through water-table feedback. Nature Geoscience 1, 763–766.

612 Jahnke, L.L., Summons, R.E., Hope, J.M., Des Marais, D.J., 1999. Carbon isotopic fractionation in
613 lipids from methanotrophic bacteria II: The effects of physiology and environmental parameters on
614 the biosynthesis and isotopic signatures of biomarkers. Geochimica et Cosmochimica Acta 63, 79–93.

615 Jauhiainen, J., Takahashi, H., Heikkinen, J.E.P., Martikainen, P.J., Vasander, H., 2005. Carbon fluxes

from a tropical peat swamp forest floor. Global Change Biology 11, 1788–1797.

Jones, M.C., Peteet, D.M., Sambrotto, R., 2010. Late-glacial and Holocene ^{15}N and ^{13}C variation from a Kenai Peninsula, Alaska peatland. Palaeogeography, Palaeoclimatology, Palaeoecology 293, 132–143.

Kluber, L.A., Johnston, E.R., Allen, S.A., Hendershot, J.N., Hanson, P.J., Schadt, C.W., 2020. Constraints on microbial communities, decomposition and methane production in deep peat deposits. PloS one 15, e0223744.

Kröpelin, S., Verschuren, D., Lézine, A.-M., Eggermont, H., Cocquyt, C., Francus, P., Cazet, J.-P., Fagot, M., Rumes, B., Russell, J.M., Darius, F., Conley, D.J., Schuster, M., von Suchodoletz, H., Engstrom, D.R., 2008. Climate-driven ecosystem succession in the Sahara: the past 6000 years. Science 320, 765–768.

Kuhry, P., Vitt, D.H., 1996. Fossil carbon/nitrogen ratios as a measure of peat decomposition. Ecology 77, 271–275.

Kurnianto, S., Warren, M., Talbot, J., Kauffman, B., Murdiyarso, D., Frolking, S., 2015. Carbon accumulation of tropical peatlands over millennia: a modeling approach. Global change biology 21, 431–444.

Lafargue, E., Marquis, F., Pillot, D., 1998. Rock-Eval 6 applications in hydrocarbon exploration, production, and soil contamination studies. Revue de l'institut français du pétrole 53, 421–437.

Lane, C.S., Mora, C.I., Horn, S.P., Orvis, K.H., 2008. Sensitivity of bulk sedimentary stable carbon isotopes to prehistoric forest clearance and maize agriculture. Journal of Archaeological Science 35, 2119–2132.

Lebamba, J., Vincens, A., Lézine, A.-M., Marchant, R., Buchet, G., 2016. Forest-savannah dynamics on the Adamawa plateau (Central Cameroon) during the "African humid period" termination: A new high-resolution pollen record from Lake Tizong. Review of Palaeobotany and Palynology 235, 129–139.

Letouzey, R., 1958. Phytogéographie camerounaise, in: Atlas du Cameroun. IRCAM, Yaoundé, p. 6.

Liu, X.-L., Leider, A., Gillespie, A., Gröger, J., Versteegh, G.J., Hinrichs, K.-U., 2010. Identification of polar lipid precursors of the ubiquitous branched GDGT orphan lipids in a peat bog in Northern Germany. Organic Geochemistry 41, 653–660.

Makou, M., Eglinton, T., McIntyre, C., Montluçon, D., Antheaume, I., Grossi, V., 2018. Plant wax n-alkane and n-alkanoic acid signatures overprinted by microbial contributions and old carbon in meromictic lake sediments. Geophysical Research Letters 45, 1049–1057.

Maley, J., Brenac, P., 1998. Vegetation dynamics, palaeoenvironments and climatic changes in the forests of western Cameroon during the last 28,000 years BP. Review of Palaeobotany and Palynology 99, 157–187.

Meyers, P.A., Lallier-Vergès, E., 1999. Lacustrine sedimentary organic matter records of Late Quaternary paleoclimates. Journal of Paleolimnology 21, 345–372.

Moore, P.D., 1989. The ecology of peat-forming processes: a review. International Journal of Coal Geology 12, 89–103.

Moreau, C., Caffy, I., Comby, C., Delqué-Količ, E., Dumoulin, J., Hain, S., Quiles, A., Setti, V., Souprayen, C., Thellier, B., Vincent, J., 2013. Research and development of the Artemis 14C AMS Facility: status report. Radiocarbon 55, 331–337.

Naafs, B., Inglis, G., Blewett, J., McClymont, E.L., Lauretano, V., Xie, S., Evershed, R., Pancost, R., 2019. The potential of biomarker proxies to trace climate, vegetation, and biogeochemical processes in peat: A review. Global and Planetary Change 179, 57–79.

Ngos III, S., Giresse, P., Maley, J., 2003. Palaeoenvironments of Lake Assom near Tibati (south Adamawa, Cameroon). What happened in Tibati around 1700 years BP? Journal of African Earth Sciences 37, 35–45.

Nguetsop, V., Bentaleb, I., Favier, C., Martin, C., Bietrix, S., Giresse, P., Servant-Vildary, S., Servant, M., 2011. Past environmental and climatic changes during the last 7200 cal yr BP in Adamawa plateau (Northern-Cameroun) based on fossil diatoms and sedimentary carbon isotopic records from Lake Mbalang. Climate of the Past 7, 1371–1393.

Nichols, J.E., Walcott, M., Bradley, R., Pilcher, J., Huang, Y., 2009. Quantitative assessment of precipitation seasonality and summer surface wetness using ombrotrophic sediments from an Arctic Norwegian peatland. Quaternary Research 72, 443–451.

Njagi, D.M., Routh, J., Olago, D., Gayantha, K., 2021. A multi-proxy reconstruction of the late Holocene climate evolution in the Kapsabet Swamp, Kenya (East Africa). Palaeogeography, Palaeoclimatology, Palaeoecology 574, 110475.

N'nanga, A., Nguetsop, V.F., Tematio, P., Ngos III, S., 2021. Paleoclimate implication on the Lake Fonjak level changes (Adamawa Plateau, Central Cameroon) during the last 13,500 cal yr BP. Journal of African Earth Sciences 182, 104286.

Page, S., Rieley, J., Shotyk, Ø., Weiss, D., 1999. Interdependence of peat and vegetation in a tropical peat swamp forest. Philosophical Transactions of the Royal Society of London. Series B: Biological Sciences 354, 1885–1897.

Pancost, R.D., Baas, M., van Geel, B., Sinninghe Damsté, J.S., 2003. Response of an ombrotrophic bog to a regional climate event revealed by macrofossil, molecular and carbon isotopic data. The Holocene 13, 921–932.

Price, G.D., McKenzie, J.E., Pilcher, J.R., Hoper, S.T., 1997. Carbon-isotope variation in Sphagnum from hummock-hollow complexes: implications for Holocene climate reconstruction. The Holocene 7, 229–233.

Roehm, C.L., 2005. Respiration in wetland ecosystems. Respiration in aquatic ecosystems 83–102.

Rosenthal, Y., Lohmann, G.P., 2002. Accurate estimation of sea surface temperatures using dissolution-corrected calibrations for Mg/Ca paleothermometry. Paleoceanography 17, 16–1.

Sachse, D., Billault, I., Bowen, G.J., Chikaraishi, Y., Dawson, T.E., Feakins, S.J., Freeman, K.H., Magill, C.R., McInerney, F.A., Van Der Meer, M.T.J., Polissar, P., Robins, R.J., Sachs, J.P., Schmidt, H.-L., Sessions, A.L., White, J.W.C., West, J.B., Kahmen, A., 2012. Molecular paleohydrology: interpreting the hydrogen-isotopic composition of lipid biomarkers from photosynthesizing organisms. Annual Review of Earth and Planetary Sciences 40, 221–249.

Saenger, A., Cécillon, L., Sebag, D., Brun, J.-J., 2013. Soil organic carbon quantity, chemistry and thermal stability in a mountainous landscape: A Rock–Eval pyrolysis survey. Organic Geochemistry 54, 101–114.

Schrag, D.P., DePaolo, D.J., Richter, F.M., 1995. Reconstructing past sea surface temperatures: Correcting for diagenesis of bulk marine carbonate. Geochimica et Cosmochimica Acta 59, 2265–2278.

Sebag, D., Disnar, J.-R., Guillet, B., Di Giovanni, C., Verrecchia, E.P., Durand, A., 2006. Monitoring organic matter dynamics in soil profiles by 'Rock-Eval pyrolysis': bulk characterization and quantification of degradation. European journal of soil science 57, 344–355.

Sebag, D., Verrecchia, E., Cécillon, L., Adatte, T., Albrecht, R., Aubert, M., Bureau, F., Cailleau, G., Copard, Y., Decaens, T., Disnar, J.-R., Hetényi, M., Nyilas, T., Trombino, L., 2016. Dynamics of soil organic matter based on new Rock-Eval indices. Geoderma 284, 185–203.

Shimamura, T., Momose, K., 2007. Reciprocal interactions between carbon storage function and plant species diversity in a tropical peat swamp forest. Asian and African area studies 6, 279–296.

Skrzypek, G., Jezierski, P., Szynkiewicz, A., 2010. Preservation of primary stable isotope signatures of peat-forming plants during early decomposition—observation along an altitudinal transect. Chemical Geology 273, 238–249.

Strobel, P., Kasper, T., Frenzel, P., Schittek, K., Quick, L., Meadows, M., Mäusbacher, R., Haberzettl, T., 2019. Late Quaternary palaeoenvironmental change in the year-round rainfall zone of South Africa derived from peat sediments from Vankervelsvlei. Quaternary Science Reviews 218, 200–214.

Sukumar, R., Ramesh, R., Pant, R., Rajagopalan, G., 1993. A ^{13}C record of late Quaternary climate change from tropical peats in southern India. Nature 364, 703–706.

Talbot, M.R., Johannessen, T., 1992. A high resolution palaeoclimatic record for the last 27,500 years in tropical West Africa from the carbon and nitrogen isotopic composition of lacustrine organic matter. Earth and Planetary Science Letters 110, 23–37.

Upton, A., Vane, C.H., Girkin, N., Turner, B.L., Sjögersten, S., 2018. Does litter input determine carbon storage and peat organic chemistry in tropical peatlands? Geoderma 326, 76–87.

Vincens, A., Buchet, G., Servant, M., and ECOFIT Mbalang collaborators, 2010. Vegetation response to the "African Humid Period" termination in Central Cameroon (7° N)–new pollen insight from Lake Mbalang. Climate of the Past 6, 281–294.

Wang, J.J., Dodla, S.K., DeLaune, R.D., 2015. Characteristics and Functions of Labile Organic Carbon in Coastal Wetland Soils of the Mississippi River Deltaic Plain, in: Labile Organic Matter—Chemical Compositions, Function, and Significance in Soil and the Environment. John Wiley & Sons, Ltd, pp. 315–336.

Wang, Z., Liu, S., Huang, C., Liu, Y., Bu, Z., 2017. Impact of land use change on profile distributions of organic carbon fractions in peat and mineral soils in Northeast China. Catena 152, 1–8.

Wei, G., Xie, L., Sun, Y., Lu, Y., Liu, Y., 2012. Major and trace elements of a peat core from Yunnan, Southwest China: implications for paleoclimatic proxies. Journal of Asian Earth Sciences 58, 64–77.

Weijers, J.W., Schouten, S., Hopmans, E.C., Geenevasen, J.A., David, O.R., Coleman, J.M., Pancost, R.D., Sinninghe Damsté, J.S., 2006. Membrane lipids of mesophilic anaerobic bacteria thriving in peats have typical archaeal traits. Environmental Microbiology 8, 648–657.

Weijers, J.W., Schouten, S., van der Linden, M., van Geel, B., Sinninghe Damsté, J.S., 2004. Water table related variations in the abundance of intact archaeal membrane lipids in a Swedish peat bog. FEMS microbiology letters 239, 51–56.

Westrich, J.T., Berner, R.A., 1984. The role of sedimentary organic matter in bacterial sulfate reduction: The G model tested 1. Limnology and oceanography 29, 236–249.

Whiticar, M.J., 1999. Carbon and hydrogen isotope systematics of bacterial formation and oxidation

of methane. Chemical Geology 161, 291–314.

Figure captions

Fig. 1: Evolution of carbon mass and carbon concentration with time in OM-dominated sediment reflecting the progressive mineralization of organic matter. Labile compounds are richer in heteroatoms than resistant compounds, leading to an increase in C concentration as labile compounds decompose while the global mass of carbon decreases.

Fig. 2: Description of the different steps of the procedure from raw to residual data.

Fig. 3: Normalized data of the NGaoundaba peat deposit plotted against age (ka cal BP & normalized): (A) TOC, (B) $\delta^{13}C_{bulk}$ and (C) C/N. The light colored curves represent the curve fitting based on the whole dataset and the dark colored curves represent the curve fitting based on the partial dataset using only depth with a positive derivative. The function selected for each parameter is indicated on the left of each panel, the constants a, b, c and d are fitted for each parameter and x-range. The selected x-range for each parameter is indicated in dark color (encircled points). The x-range limit is indicated in both age and depth for each parameter.

Fig. 4: Age-depth model of NGaoundaba peatland core. The corresponding section number is indicated for each ^{14}C sample.

Fig. 5: Raw data (i.e., before data processing) from the NGaoundaba peat deposit: (A) TOC (%), (B) $\delta^{13}C_{bulk}$ (‰), (C) C/N from Elemental and stable isotope analysis and the I-index from Rock-Eval® analysis. Visible transitions are indicated with vertical red dashed lines.

Fig. 6: Retreated NGaoundaba peat deposit data and regional climatic and environmental settings: (A) Insolation 0°N ($W.m^{-2}$) from Berger et al. (1981), (B) $\delta D_{n\text{-}alkC31}$ corrected for vegetation changes in Lake Barombi (Southwest Cameroon) (Garcin et al., 2018), (C) Simplified pollen data from Lake MBalang (about 25 km from the NGaoundaba peat deposit) (Vincens et al., 2010) (D) TOC (%), (E) $\delta^{13}C_{bulk}$ (‰) and (F) C/N as well as (G) Hydrogen Index (HI) from Rock-Eval® analysis. The African Humid Period is highlighted in green, the termination of this period has been represented as a color gradient to illustrate the uncertainties and different possible timings of the termination. The mean

value of HI is indicated as a dashed line. Visible transitions are indicated with vertical red dashed lines.

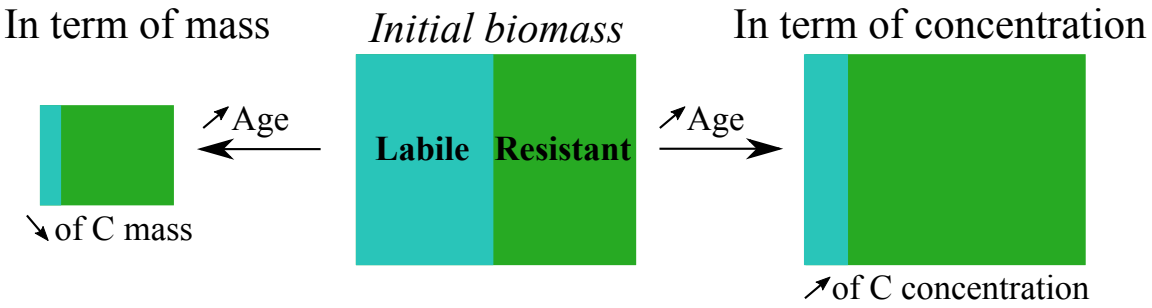
In term of mass
Initial biomass
In term of concentration
Age
Labile
Resistant
Age
of C mass
of C concentration

Fig. 1:

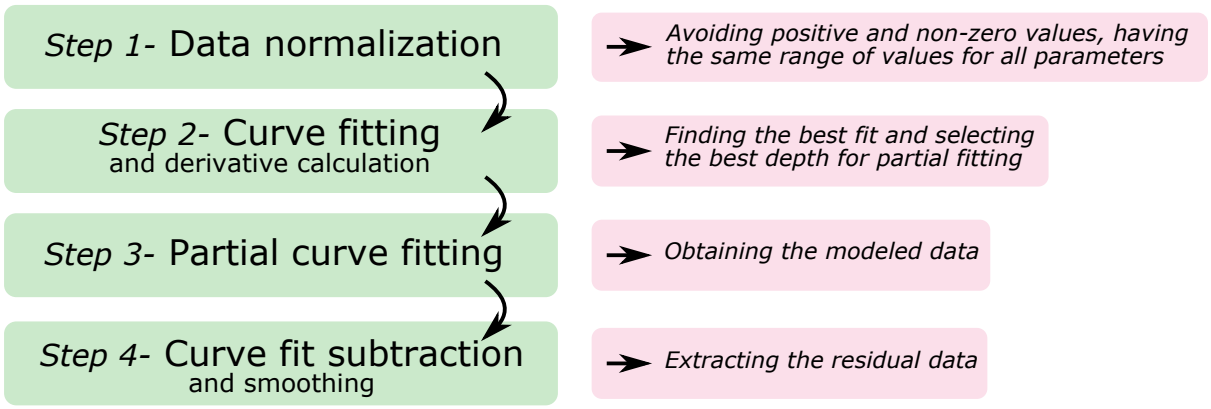
Step 1- Data normalization
Avoiding positive and non-zero values, having the same range of values for all parameters
Step 2- Curve fitting
and derivative calculation
Finding the best fit and selecting the best depth for partial fitting
Step 3- Partial curve fitting
Obtaining the modeled data
Step 4- Curve fit subtraction
and smoothing
Extracting the residual data

Fig. 2:

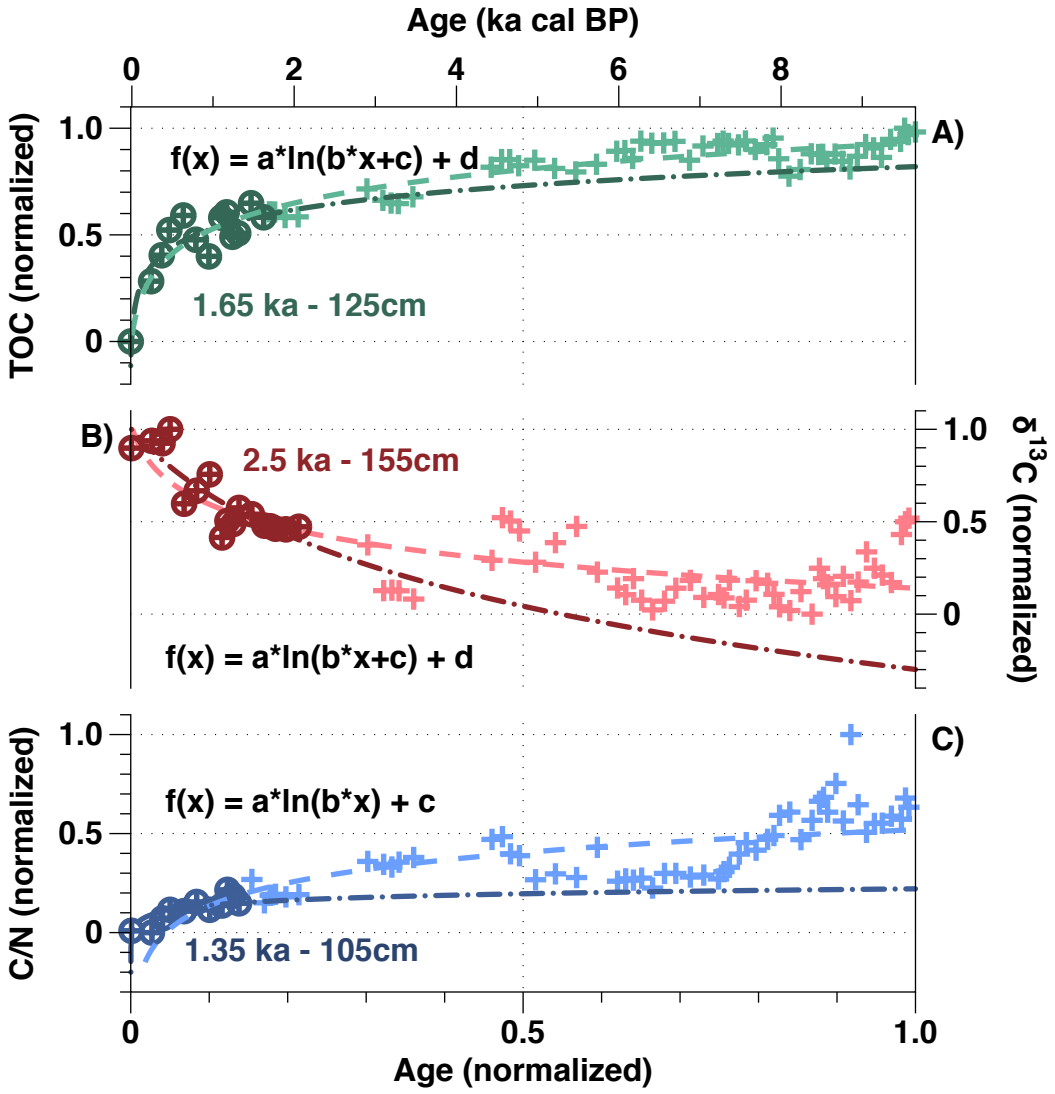
Age (ka cal BP)
0
2
4
6
8
TOC (normalized)
1.0
0.5
0
A)
f(x) = a*ln(b*x+c) + d
1.65 ka - 125cm
B)
2.5 ka - 155cm
f(x) = a*ln(b*x+c) + d
δ13C (normalized)
C/N (normalized)
C)
f(x) = a*ln(b*x) + c
1.35 ka - 105cm
Age (normalized)

Fig. 3:

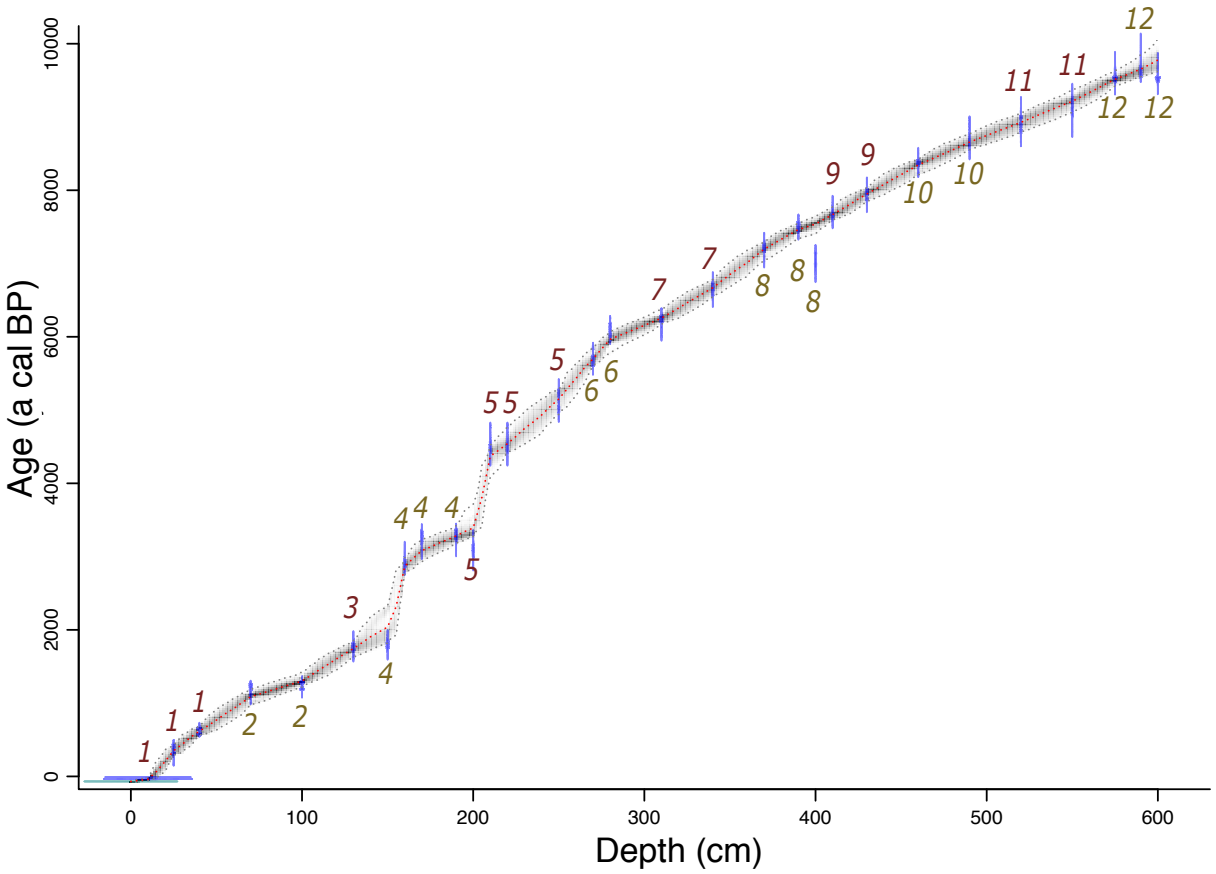
Age (a cal BP)
0
2000
4000
6000
8000
10000
0
100
200
300
400
500
600
Depth (cm)

Fig. 4:

Sample code	Depth (cm)	Uncalibrated Age	Calibrated age (a cal BP)
58976	10	120 pMC	-39
62587	25	330 ± 30 BP	343
58977	40	725 ± 30 BP	614
58978	70	1310 ± 30 BP	1093
58979	100	1390 ± 30 BP	1290
58980	130	1870 ± 30 BP	1741
62588	150	1910 ± 30 BP	1981
64844	160	2840 ± 30 BP	2871
58981	170	3090 ± 30 BP	3082
58982	190	3130 ± 30 BP	3274
62589	200	2975 ± 30 BP	3345
64845	210	4070 ± 30 BP	4417
58983	220	4070 ± 30 BP	4531
58984	250	4475 ± 30 BP	5180
62590	270	5000 ± 35 BP	5690
58985	280	5335 ± 30 BP	5960
58986	310	5460 ± 30 BP	6255
58987	340	5875 ± 30 BP	6668
58988	370	6335 ± 35 BP	7201
64846	390	6660 ± 30 BP	7465
58989	400	6170 ± 30 BP	7547
62591	410	6870 ± 40 BP	7665
58990	430	7180 ± 40 BP	7955
58991	460	7600 ± 35 BP	8361
58992	490	7925 ± 40 BP	8653
58993	520	8080 ± 35 BP	8926
58994	550	8210 ± 40 BP	9223
62592	575	8605 ± 45 BP	9511
64847	590	8700 ± 40 BP	9642
58995	600	8590 ± 40 BP	9759

Table 1: Chronology of NGaoundaba peatland with uncalibrated AMS ^{14}C ages (BP : before present) and calibrated median ^{14}C age (a cal BP).

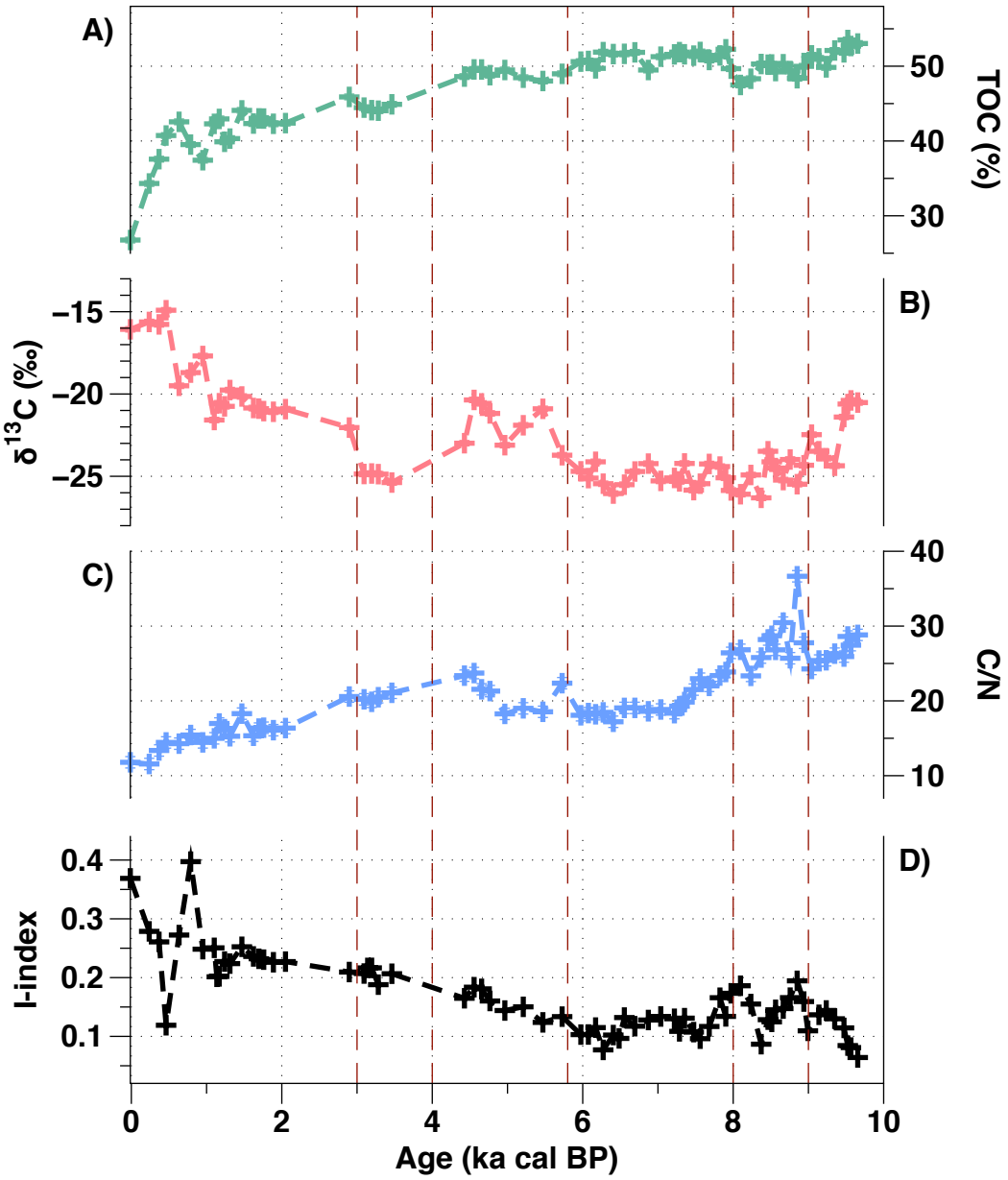

893

894 **Fig. 5:**

895

896

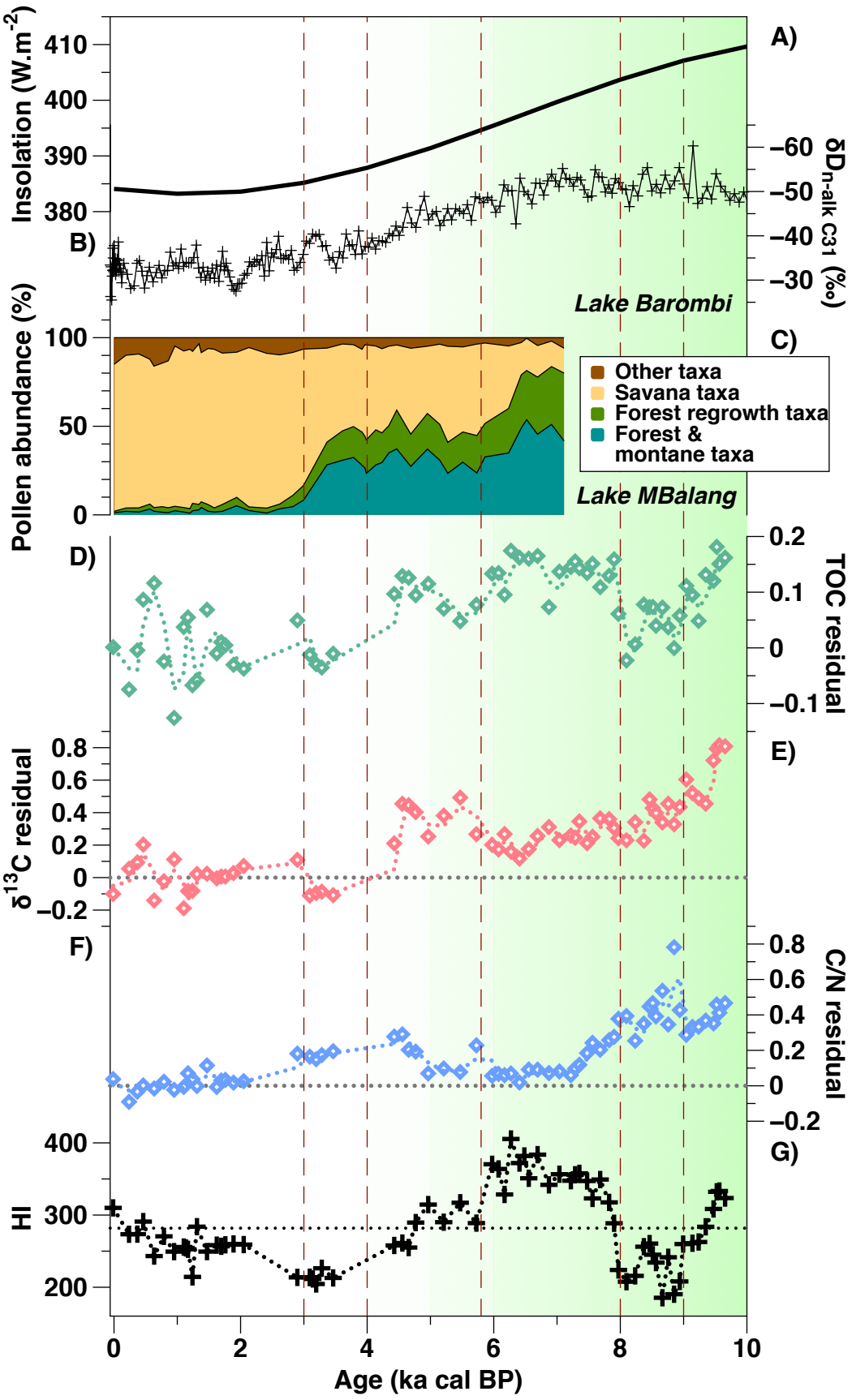

897

898 **Fig. 6:**

899